

# VELOCITY GRADIENT TENSOR ANALYSIS FOR TURBULENCE REFORMULATED IN TERMS OF NORMAL AND NON-NORMAL CONTRIBUTIONS

**Chris J. Keylock**

School of Architecture, Building and Civil Engineering  
Loughborough University  
Loughborough, LE11 3TU, U.K.  
c.j.keylock@lboro.ac.uk

## ABSTRACT

Making use of a recently proposed, Schur decomposition approach to the analysis of the velocity gradient tensor (VGT), we provide a preliminary study of the resulting new terms for the case of a turbulent channel flow in the outer part of the logarithmic region. Previously, this approach has only been used for homogeneous, isotropic turbulence (HIT). In particular, we define six regions in the space of the second and third invariants of the tensor (the Q-R diagram) and condition our analysis on these regions and if the flow is undergoing a significant ejection or sweep event. When comparing the tendency for the VGT to form rod-like or disc-like structures, the results are very close to those for HIT. However, that the differences between ejections and sweeps are greater than this in the regions where Q and R are negative indicates a topological difference of potential significance for dissipation modelling. Where Q and R are negative, but the VGT's eigenvalues are complex we find a particularly strong tendency for the dynamics to be dominated by the non-normal contribution to the second order terms. In the more strongly vortical regions, the non-normal contribution to the sweeps is greater than for the ejections.

## INTRODUCTION

Studies of the velocity gradient tensor (VGT) for incompressible turbulent flows have revealed that the joint probability distribution function for the second (Q) and third (R) invariants of the tensor appear to have universal characteristics when the turbulence is fully developed (Chacin & Cantwell, 2000; Gomes-Fernandes *et al.*, 2014; Buxton *et al.*, 2017) and an example distribution function is provided in Fig. 1. Understanding the dynamics that lead to this distribution is an important pathway for developing new closures for large-eddy simulations (Biferale *et al.*, 2007; Wilczek & Meneveau, 2014) and much of this previous work has been reviewed by Meneveau (2011). While the Q-R diagram clearly contains significant information on turbulence, the second invariant represents the difference between enstrophy and total strain, and the third invariant the difference between strain production and enstrophy production, and there are significant dynamical effects associated with these individual terms (?). What is not clear at present is how these latter processes vary for different flows, and how local and non-local effects contribute to these dynamics. This is an important research question because dif-

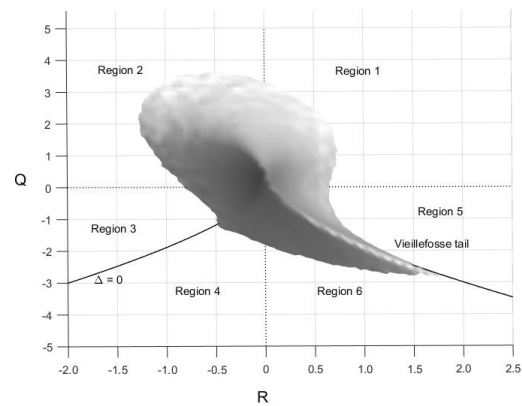


Figure 1. The joint probability distribution function for the second (Q) and third (R) invariants of the velocity gradient tensor, including the discriminant,  $\Delta = 0$ , and the typology for the six regions adopted in this study. The distinctive Vieillefosse tail (Vieillefosse, 1984) is also highlighted.

ferent forcings introduce different vortex interactions (Nagata *et al.*, 2013), influencing the nature of the non-local contributions and, thus, dissipation (Vassilicos, 2015).

One of the most important flows to consider from a practical perspective is a channel flow as the autogenic generation of flow structures near the wall (Zhou *et al.*, 1999) results in a potential complexity to these small-scale processes, the understanding of which can enhance applied modelling methods (such as large-eddy simulation closures). The first study to consider the Q-R dynamics of a turbulent boundary-layer in detail was that by Chacin & Cantwell (2000). It was found that the ejection and sweep events occurred preferentially along the Vieillefosse tail seen in Fig. 1, while the more strongly persistent vortical structures were relatively passive in terms of the wall dynamics.

Recently, a Schur decomposition of the velocity gradient tensor has been introduced and the additional terms that result studied for the case of homogeneous, isotropic turbulence (Keylock, 2018). Here we provide some initial results on the examination of these terms for a direct numerical simulation of a channel flow.

## KEY CONCEPTS

Taking the spatial derivative of the Navier-Stokes equations leads to an evolution equation for the velocity gradient tensor (VGT),  $A$ , for turbulence. Defining  $A_{ij} = \partial u_i / \partial x_j$ , the strain,  $S_A$ , and rotation,  $\Omega_A$ , may be evaluated directly

$$S_A = \frac{1}{2}(A + A^T) \quad (1)$$

$$\Omega_A = \frac{1}{2}(A - A^T) \quad (2)$$

where the ‘T’ superscript indicates a transpose. The characteristic equation for  $A$  is

$$\lambda_i^3 + P\lambda_i^2 + Q\lambda_i + R = 0 \quad (3)$$

and incompressibility means that the first invariant,  $P = 0$ , leaving the second and third invariants, which are traditionally expanded in terms of  $S_A$  and  $\Omega_A$  as

$$Q = \frac{1}{2}(\|\Omega_A\|^2 - \|S_A\|^2) \\ R = -\det(S_A) - \text{tr}(\Omega_A^2 S_A) \quad (4)$$

where  $\|\dots\|$  is the Frobenius norm. The primary disadvantage of an eigenvalue-based analysis of the VGT is that it is not an additive decomposition of the tensor, in contrast to  $A = S_A + \Omega_A$ , with residual information left in the non-unitary eigenvectors. However, an additive decomposition may be accomplished by using the Schur decomposition (Schur, 1909), which imposes a unitary structure on the rotation matrix

$$A = UTU^T \\ T = L + N \quad (5)$$

where  $L$  is a diagonal matrix of eigenvalues,  $L_{ii} = \lambda_i$ , and  $N$  is (block) upper triangular and contains the non-normal components of the tensor, such that the Frobenius norm of  $N$ ,  $\|N\|$ , is a well-known measure of matrix non-normality (Henrici, 1962). This then leads to an additive decomposition,  $A = B + C$ , where  $B = ULU^T$  and  $C = UNU^T$ , from which it is possible to obtain corresponding strain and rotation tensors (Keylock, 2018).

Evolution equations for the invariants can be written only in terms of each other if the non-normal contributions to the tensorial dynamics (from viscosity and the deviatoric part of the pressure Hessian) are ignored (Cantwell, 1992), it follows that we can write

$$Q = \frac{1}{2}(\|\Omega_B\|^2 - \|S_B\|^2) \\ R = -\det(S_B) - \text{tr}(\Omega_B^2 S_B) \quad (6)$$

However, as, for example,  $\|S_A\|^2 \neq \|S_B\|^2$  in general, it follows that terms that contribute to each invariant are eliminated when the differences in (4) are taken. The missing term for the normal enstrophy and normal total strain is the non-normality  $\|\Omega_C\|^2$  such that,

$$\|S_A\|^2 = \|S_B\|^2 + \|\Omega_C\|^2 \\ \|\Omega_A\|^2 = \|\Omega_B\|^2 + \|\Omega_C\|^2 \quad (7)$$

For the equation for the third invariant, there are two new terms, which appear in both the expressions for strain production and enstrophy production

$$-\det(S_A) = -\det(S_B) + \text{tr}(\Omega_C^2 S_B) - \det(S_C) \\ \text{tr}(\Omega_A^2 S_A) = \text{tr}(\Omega_B^2 S_B) + \text{tr}(\Omega_C^2 S_B) - \det(S_C) \quad (8)$$

where, from left to right, the strain production is given by the sum of the normal strain production, the interaction production and the non-normal production, and the enstrophy production is the sum of the normal enstrophy production, the interaction production and the non-normal production.

The second consequence of our approach is the definition of rotation and, thus, enstrophy. In a Lagrangian frame, the existence of a conjugate pair of eigenvalues means that there is a closed streamline (and, thus, a vortex according to swirl-based measures of flow structure Zhou *et al.* (1999)). This fact is explicit in our formulation because  $\|\Omega_B\| = 0$  if  $\Delta \leq 0$  where  $\Delta = Q^3 + (27/4)R^2$  is the discriminant function such that a conjugate pair of eigenvalues for the VGT arises when  $\Delta > 0$ . In other words, when all the eigenvalues of the VGT are real,  $Q = -0.5\|S_B\|^2$  and  $R = -\det(S_B)$ . Related to this is the advantage that arises from the  $A = B + C$  decomposition when considering the straining behaviour of the tensor: the sign of  $R$  dictates the signs for  $-\det(S_B)$  and  $\text{tr}(\Omega_B^2 S_B)$ , with  $R > 0$  resulting in  $-\det(S_B) > 0$  and  $\text{tr}(\Omega_B^2 S_B) < 0$ . Given that no such constraint exists on the signs for  $-\det(S_A)$  and  $\text{tr}(\Omega_A^2 S_A)$ , deviations from this pattern highlight the importance of one or both of the interaction production and non-normal production terms in (8).

In this paper we apply this framework to the case of turbulent channel flow, relative to the behaviour for homogeneous isotropic turbulence that we have studied previously (Keylock, 2018).

## TURBULENT CHANNEL FLOW SIMULATION

The simulation we have used in this work is that by Graham *et al.* (2016) based on the simulation by Lee & Moser (2015) and is stored as part of the Johns Hopkins Turbulence Database (Li *et al.*, 2008). The domain size is  $8\pi h \times 2h \times 3\pi h$  where  $h$  is the channel half height. The bulk velocity is  $U_b = 0.99994$ , the kinematic viscosity is  $\nu = 5 \times 10^{-5}$ , and the shear velocity is  $u_\tau = 4.9968 \times 10^{-2}$ , giving a friction velocity Reynolds number of  $\text{Re}_\tau = u_\tau h / \nu \sim 1000$ . We focussed on a region with longitudinal and transverse dimensions of  $\pi h \times \pi h$  in extent and extracted data at a resolution of  $256^2$  velocity gradient tensors in such a plane. We concentrated on the logarithmic part of the velocity profile by extracting 256 of these planes at evenly spaced distances from  $70 \leq y^+ \leq 350$  in the outer region of the logarithmic region of the velocity profile, where the plus indicates that wall units are adopted. Extracted velocity gradients were non-dimensionalized using  $u_\tau^2 / \nu$ .

## RESULTS

Here we focus on three properties of the VGT in the channel flow: the nature of the strain eigenvalues and the tendency for the flow to behave in a disc-like or rod-like fashion, and then the typical depth averaged values of the terms that feature in (7) and (8) as a function of region of the Q-R diagram and whether or not an ejection or sweep is occurring.

## Straining Structure

It was clear from early simulations of turbulent flow fields that there was a tendency for the strain tensor,  $S_A$ , to have two positive eigenvalues, meaning that turbulence preferentially forms disc-like rather than rod-like structures (Kerr, 1985; Ashurst *et al.*, 1987; Li & Meneveau, 2007). An effective index to investigate this is that due to Lund & Rogers (1994):

$$e_{LR}^{(A)} = \frac{-3\sqrt{6}\det(S_A)}{\text{tr}(S_A^2)^{\frac{3}{2}}} \quad (9)$$

where  $-1 < e_{LR}^{(A)} < 1$ . However, it follows from (8) that this index may be expanded in a similar fashion to give  $e_{LR}^{(A)} = e_{LR}^{(B)} + e_{LR}^{(I)} + e_{LR}^{(C)}$  (Keylock, 2018), where the superscripts ‘B’ and ‘C’ indicate which strain tensor is applied in the numerator of (9), and

$$e_{LR}^{(I)} = \frac{-3\sqrt{6}\text{tr}(\Omega_C^2 S_B)}{\text{tr}(S_A^2)^{\frac{3}{2}}} \quad (10)$$

Figure 2 gives the mean values for these indices as a function of height and region of the Q – R diagram. There is little vertical variation over this range of  $y^+$  and all the values shown are within 0.019 of the equivalents for homogeneous isotropic turbulence we have reported previously (Keylock, 2018). The necessary condition that  $R > 0$  (red lines) correspond to positive values for  $e_{LR}^{(B)}$  and negative values are associated with  $R < 0$  (blue lines) is clear from panel (b). What is particularly clear is how this decomposition explains the dominance of the disc-shaped topology when, based on the relative occupancy of the different regions of the Q – R diagram and a focus on the local contribution,  $e_{LR}^{(B)}$ , one would expect discs to favour rods in the approximate ratio of 55:45. However, that  $\langle e_{LR}^{(I)} \rangle$  is positive in all regions except region 1 and is particularly positive in regions 2 and 3, where  $e_{LR}^{(B)} < 0$  explains why this disc-like nature to the flow arises, with the weakly positive contribution of  $\langle e_{LR}^{(C)} \rangle$  of secondary importance to the average results.

Both regions close to the Vieillefosse tail have  $\langle e_{LR}^{(A)} \rangle \sim 0.6$ , but the value in region 1 is close to zero. While  $\langle e_{LR}^{(B)} \rangle$  is less strongly positive than for regions 5 and 6, the crucial factor explaining this behaviour is the negative value for  $\langle e_{LR}^{(I)} \rangle$ , which is unique to this region. Thus, the action of normal straining on the non-local enstrophy results in a stretching action that is of sufficient magnitude to almost completely overcome, in the mean, the compressive action of the normal straining on the normal enstrophy. As a consequence, the two regions with  $Q > 0$  both typically have a strong misalignment between the orientation of  $\Omega_B$  and  $\Omega_C$  such that the action of  $S_B$  has an opposite effect when applied to each component of the enstrophy. However, in the case of region 1 these two effects are approximately equal and opposite ( $\langle e_{LR}^{(B)} \rangle \sim 0.11$ ,  $\langle e_{LR}^{(I)} \rangle \sim -0.14$ ), while in region 2  $\langle e_{LR}^{(A)} \rangle \sim 0.33$  as a consequence of  $\langle e_{LR}^{(B)} \rangle \sim -0.12$ ,  $\langle e_{LR}^{(I)} \rangle \sim 0.35$  and  $\langle e_{LR}^{(C)} \rangle \sim 0.1$ .

Reynolds averaging of the Navier-Stokes equations leads to a Reynolds stress tensor given by  $\tau_R = -\rho u_i' u_j'$ . In a

boundary-layer the dominant shear term involves the longitudinal and vertical velocity components, and the joint probability distribution function for these terms may be disaggregated into quadrants (Bogard & Tiederman, 1986; Keylock *et al.*, 2014), where the most significant occurrences are those that contribute positively to the Reynolds stress: the ejections (quadrant 2) and sweeps (quadrant 4). The application of quadrant analysis commonly involves the use of a threshold hole size, expressed in terms of the standard deviation,  $\sigma(\dots)$ , of the velocity components. In this study we use a hole size of 2. That is, a quadrant occurs when  $|u_i' u_j'| > 2\sigma_i \sigma_j$ .

Given that none of the results for  $e_{LR}^{(A)}$  in Fig. 2 differ from those for HIT by more than 0.019, the differences between ejections and sweeps in Fig. 3 appear to have some significance, particularly for regions 3 and 4 of the Q-R diagram. It is the normal contribution,  $e_{LR}^{(B)}$  that appears to be the most important contributing term, and this has negative values in these regions, meaning that the sweeps are the events with the more rod-like topology in these regions. Given that it is vortex compression that tends to lead to dissipation (Tsinober, 2001), the implication is that, in these regions in particular, conditioning the degree of dissipation in a closure model on the nature of the quadrants that constitute the Reynolds stress is advantageous as the sweeps are likely to promote less dissipation than an equilibrium model that balances production and dissipation instantaneously and locally, is likely to assume.

## The Decomposition of Q

The results in Figure 4 show the values for the 95th quantile of the distribution for each of the three terms from (7) sub-divided by the region of Q-R space and if they arise in ejection events (left-hand panels in each pair) or sweeps (right-hand panels). Note that while the relative magnitudes of total strain (red) and enstrophy (black) are necessarily a function of the rows of the diagram (because Q decreases in value from top to bottom), the Q-R diagram says nothing about the magnitude of  $\|\Omega_C\|^2$ . This term is found to dominate in three of the four cases in regions 3 and 5, particularly for the ejections in region 3. The greatest amount of normal stress arises for the ejections in region 6, while the largest normal enstrophy arises for the sweeps, with the relative difference between sweeps and ejections greatest in region 1. Hence, the term in (7) that is neglected when Q is the focus of analysis, is the most important in regions where the VGT eigenvalues are complex but total strain exceeds enstrophy.

## The Decomposition of R

Similar results for the production terms are provided in Fig. 5, the difference being that because these terms can be either positive or negative, the profile-averaged values for the 5th and 95th percentiles are shown, with a line connecting these two values. In the top row it is clear that normal enstrophy production has the greatest magnitude in regions 1 and 2, and is greater for sweeps than ejections. However, it is the ejections where the interaction production is greater on average when examining the net contribution in the same direction as the normal enstrophy. Interaction production is of particular importance to the dynamics of both types of boundary-layer event in region 3, as well as ejections in region 4, while normal strain production is dominant in both regions 5 and 6, but this is particularly the case for ejection

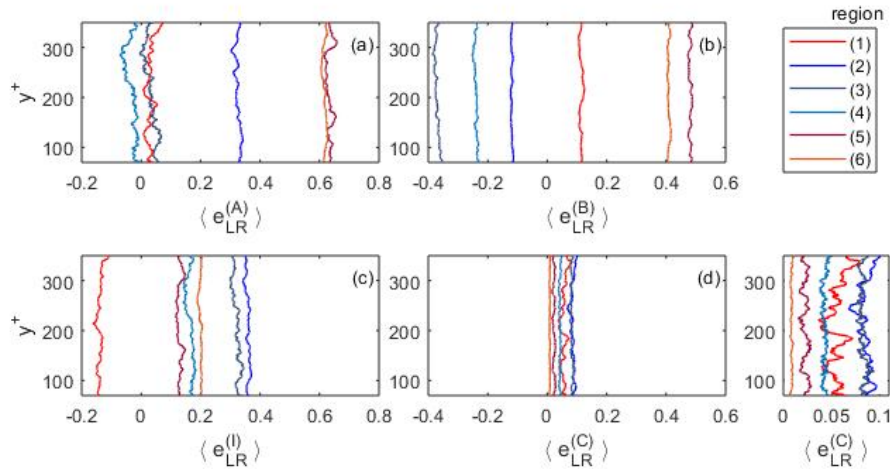


Figure 2. Profiles of the mean values for the conventional Lund & Rogers (1994) index for the strain tensor,  $S_A$  are shown in (a), with the normal contribution, interaction production contribution, and non-normal contributions given in (b), (c), and (d) respectively. An enlarged version of the latter is also shown. Results are subdivided by the six regions of the Q – R diagram, with red for positive R regions and blue for negative R.

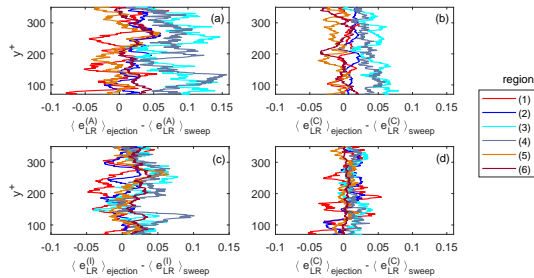


Figure 3. Profiles of the differences in mean values for the  $e_{LR}$  indices between quadrant 2 (ejections) and quadrant 4 (sweeps). Results are subdivided by the six regions of the Q – R diagram, with red for positive R regions and blue for negative R.

tions. While the non-normal production term is, on average, the term with the smallest magnitude, the range of values is comparable to  $\text{tr}(\Omega_C^2 S_B)$ , and greater than that for normal strain production in the strongly vortical regions (regions 1 and 2). This term is of greater variability in the case of the sweeps and, because of its (weak) bias towards positive values acts in the same sense of the normal enstrophy production in region 2, and in opposition in region 1. Thus the sum of these effects, seen in a traditional analysis fails to account for differences that arise because of the asymmetries in the underlying equations (normal enstrophy production is negative in region 1, 5 and 6, and positive in regions 2, 3, and 4, while the interaction production and non-normal production contributions are typically positive. By isolating these dynamical contributions, there is greater potential to examine the interplay between local and non-local processes.

## CONCLUSIONS

Adopting the Schur decomposition approach to the study of the velocity gradient tensor permits more refined analyses of turbulence dynamics as there are seven terms generated rather than four, with significant constraints on

the signs or existence of the various normal terms in different parts of the Q-R diagram. In terms of the topology of the strain tensor the differences in values between ejections and sweeps is greater in regions 3 and 4 than between the channel flow results and those for HIT, implying that these preliminary results, at the very least, indicate a topological difference between ejections and sweeps where R is negative and Q is negative. Further work is needed to demonstrate broader significance to these results, but that the  $e_{LR}^{(I)}$  term is important to these differences in topology, and that this reflects, in part, non-local contributions to the turbulence dynamics, indicates that the structure of the surrounding field is having some differential impact on the manner in which the ejection events behave relative to the sweeps. In general, the effect of the non-normal or interaction terms is greatest in region 3, and the results in the middle row of Fig. 5 justify the division of the Q-R space into six regions, rather than the four that arise when one focuses purely on topology (Chong *et al.*, 1990).

Given the work showing how the dissipation coefficient in turbulence depends on the structure of the turbulence flow field (in particular the stagnation point structure) (Goto & Vassilicos, 2009), and the work on non-equilibrium turbulence that has shown how mixing is influenced by the arrangement of vortices (Laizet & Vassilicos, 2012), isolating the non-local contributions as was done here and in our study of HIT (Keylock, 2018) should help us to understand and therefore model the role of non-local contributions on the dynamics for various forcing strategies.

## REFERENCES

- Ashurst, W. T., Kerstein, A. R., Kerr, R. A. & Gibson, C. H. 1987 Alignment of vorticity and scalar gradient with strain rate in simulated Navier-Stokes turbulence. *Phys. Fluids* **30**, 2343–2353.
- Biferale, L., Chevillard, L., Meneveau, C. & Toschi, F. 2007 Multiscale model of gradient evolution in turbulent flows. *Phys. Rev. Lett.* **98**, 214501.
- Bogard, D. G. & Tiederman, W. G. 1986 Burst detection with single-point velocity measurements. *J. Fluid Mech.* **162**, 389–413.

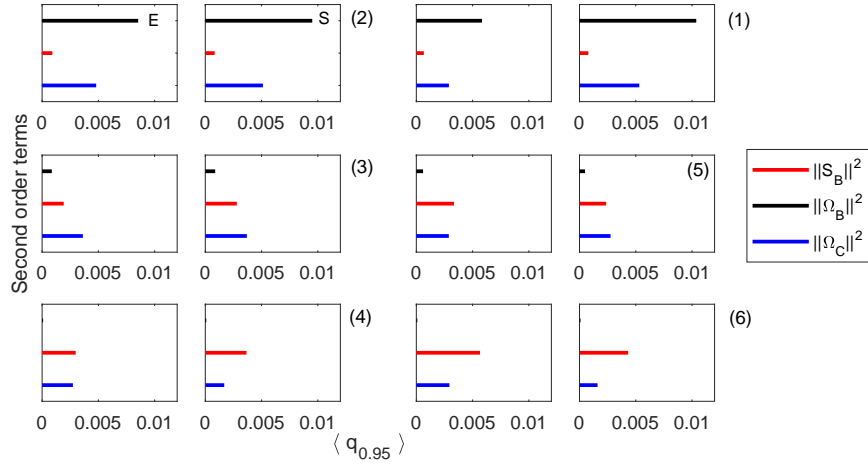


Figure 4. The vertically averaged values for the 95th percentiles of  $\|S_B\|^2$ ,  $\|\Omega_B\|^2$ , and  $\|\Omega_C\|^2$  for each region of the Q-R diagram and for ejections and sweeps.

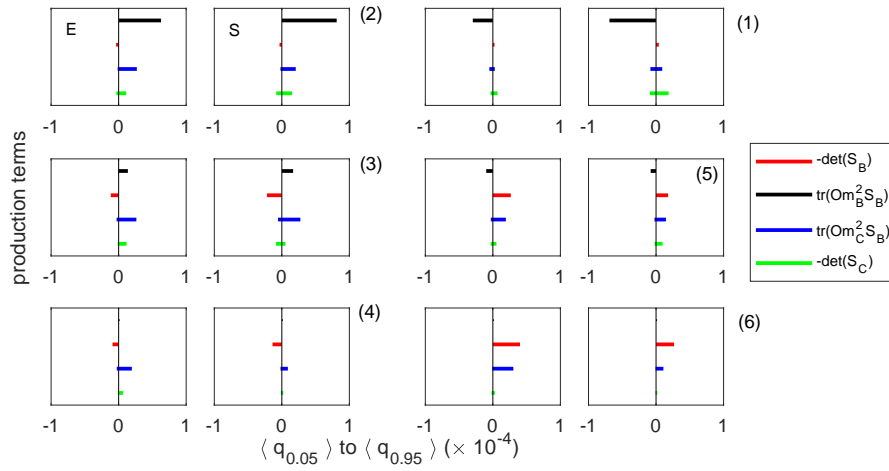


Figure 5. The vertically averaged values for the 5th and 95th percentiles of  $-\det(S_B)$ ,  $\text{tr}(\Omega_B^2 S_B)$ ,  $\text{tr}(\Omega_C^2 S_B)$ , and  $-\det(S_C)$  for each region of the Q-R diagram and for ejections and sweeps.

Buxton, O. R. H., Breda, M. & Chen, X. 2017 Invariants of the velocity-gradient tensor in a spatially developing inhomogeneous turbulent flow. *J. Fluid Mech.* **817**, 1–20.  
 Cantwell, B. J. 1992 Exact solution of a restricted Euler equation for the velocity gradient tensor. *Phys. Fluids A* **4** (4), 782–793.  
 Chacin, J. M. & Cantwell, B. J. 2000 Dynamics of a low Reynolds number turbulent boundary layer. *J. Fluid Mech.* **404**, 87–111.  
 Chong, M. S., Perry, A. E. & Cantwell, B. J. 1990 A general classification of three-dimensional flow fields. *Phys. Fluids A* **2**, 765–777.  
 Gomes-Fernandes, R., Ganapathisubramani, B. & Vassilicos, J. C. 2014 Evolution of the velocity-gradient tensor in a spatially developing turbulent flow. *J. Fluid Mech.* **756**, 252–292.  
 Goto, S. & Vassilicos, J. C. 2009 The dissipation rate coefficient of turbulence is not universal and depends on the internal stagnation point structure. *Phys. Fluids* **21**, 035104.  
 Graham, J., Kanov, K., Yang, X. I. A., Lee, M. K., Malaya, N., Lalescu, C. C., Burns, R., Eyink, G., Szalay, A., Moser, R. D. & Meneveau, C. 2016 A web services-accessible database of turbulent channel flow and its use

for testing a new integral wall model for LES. *J. Turbulence* **17** (2), 181–215.  
 Henrici, P. 1962 Bounds for iterates, inverses, spectral variation and fields of values of non-normal matrices. *Numer. Math.* **4**, 24–40.  
 Kerr, R. M. 1985 Higher-order derivative correlations and the alignment of small-scale structures in isotropic, numerical turbulence. *J. Fluid Mech.* **153**, 31–58.  
 Keylock, C. J. 2018 The Schur decomposition of the velocity gradient tensor for turbulent flows. *J. Fluid Mech.* **848**, 876–904.  
 Keylock, C. J., Lane, S. N. & Richards, K. S. 2014 Quadrant/octant sequencing and the role of coherent structures in bed load sediment entrainment. *J. Geophys. Res.* **119**, 264–286.  
 Laizet, S. & Vassilicos, J. C. 2012 Fractal space-scale unfolding mechanism for energy-efficient turbulent mixing. *Phys. Rev. E* **86** (4), 046302.  
 Lee, M. & Moser, R. D. 2015 Direct numerical simulation of turbulent channel flow up to  $Re_\tau = 5200$ . *J. Fluid Mech.* **774**, 395–415.  
 Li, Y. & Meneveau, C. 2007 Material deformation in a restricted Euler model for turbulent flows: Analytic solution and numerical tests. *Phys. Fluids* **19**, 015104.

- Li, Y., Perlman, E., Wan, M., Yang, Y., Burns, R., Meneveau, C., Chen, S., Szalay, A. & Eyink, G. 2008 A public turbulence database cluster and applications to study Lagrangian evolution of velocity increments in turbulence. *J. Turbulence* **9** (31).
- Lund, T. S. & Rogers, M. M. 1994 An improved measure of strain state probability in turbulent flows. *Phys. Fluids* **6** (5), 1838–1847.
- Meneveau, C. 2011 Lagrangian dynamics and models of the velocity gradient tensor in turbulent flows. *Ann. Rev. Fluid Mech.* **43**, 219–245.
- Nagata, K., Sakai, Y., Inaba, T., Suzuki, H., Terashima, O. & Suzuki, H. 2013 Turbulence structure and turbulence kinetic energy transport in multiscale/fractal-generated turbulence. *Phys. Fluids* **25** (065102).
- Schur, I. 1909 Über die charakteristischen Wurzeln einer linearen Substitution mit einer Anwendung auf die Theorie der Integralgleichungen. *Math. Ann.* **66**, 488–510.
- Tsinober, A. 2001 Vortex stretching versus production of strain/dissipation. In *Turbulence Structure and Vortex Dynamics* (ed. J. C. R. Hunt & J. C. Vassilicos), pp. 164–191. Cambridge University Press.
- Vassilicos, J. C. 2015 Dissipation in turbulent flows. *Ann. Rev. Fluid Mech.* **47**, 95–114.
- Vieillefosse, P. 1984 Internal motion of a small element of fluid in an inviscid flow. *Physica A* **125**, 150–162.
- Wilczek, M. & Meneveau, C. 2014 Pressure Hessian and viscous contributions to velocity gradient statistics based on Gaussian random fields. *J. Fluid Mech.* **756**, 191–225.
- Zhou, J., Adrian, R. J., Balachandar, S. & Kendall, T. M. 1999 Mechanisms for generating coherent packets of hairpin vortices. *J. Fluid Mech.* **387**, 353–396.